Received: 25 October 2022 | Accepted: 2 December 2022

DOI: 10.1002/bmm2.12006

REVIEW

BMEMat WILEY

Piezotronic and piezo-phototronic effects on sonodynamic disease therapy

Yunchao Zhao[1,2] | **Tian Huang**[1,2] | **Xiaodi Zhang**[3] | **Yuanbo Cui**[4] | **Lili Zhang**[5] | **Linlin Li**[1,2,6] | **Zhong Lin Wang**[1,7]

[1]Beijing Institute of Nanoenergy and Nanosystems, Chinese Academy of Sciences, Beijing, China

[2]Center on Nanoenergy Research, School of Physical Science and Technology, Guangxi University, Nanning, China

[3]Department of Neurology, Institute for Cell Engineering, Johns Hopkins University School of Medicine, Baltimore, USA

[4]Santa Clara University, Santa Clara, USA

[5]HCA Florida Healthcare Westside/Northwest Hospital Internal Medicine, Plantation, USA

[6]School of Nanoscience and Technology, University of Chinese Academy of Sciences, Beijing, China

[7]Georgia Institute of Technology, Atlanta, USA

Correspondence
Linlin Li, Beijing Institute of Nanoenergy and Nanosystems, Chinese Academy of Sciences, Beijing 101400, China.
Email: lilinlin@binn.cas.cn

Funding information
Strategic Priority Research Program of the Chinese Academy of Sciences, Grant/Award Number: XDA16021103; National Natural Science Foundation of China, Grant/Award Numbers: 81471784, 82072065; National Youth Talent Support Program; Fundamental Research Funds for the Central Universities, Grant/Award Number: E2EG6802X2

Abstract

With the development of engineered nanomaterials and nanomedicines, utilization of nanomaterials to generate excessive reactive oxygen species under exogenous ultrasound (US) irradiation for realizing disease therapy, namely sonodynamic therapy (SDT), has attracted widespread attention. Compared with traditional photodynamic therapy, US shows deeper tissue penetration to reach deep-seated location. However, the development of high-efficiency sonosensitizers remains one of the gravest challenges in current related research and future clinical application. Latterly, benefiting from the piezotronic and piezo-phototronic effects, novel sonosensitizers based on piezoelectric semiconductor (PS) nanomaterials have exhibited inspiring application prospects in SDT. In this review, we outline the structures and physicochemical properties of PS nanomaterials that has potential applications in SDT, and introduce the presumed mechanisms of PS nanomaterials in SDT. Then, the latest research progress of PS nanomaterials as sonosensitizers in cancer therapy and antibacterial applications are summarized. Finally, the existing challenges and future development trends in this field are prospected.

KEYWORDS
cancer therapy, piezo-phototronic effect, piezoelectric effect, piezoelectric semiconductor, sonodynamic therapy, sonosensitizers

1 | INTRODUCTION

Reactive oxygen species (ROS) are a group of highly active oxygen-containing molecules generated from molecular oxygen (O_2) during the electron transfer process, mainly including superoxide anion ($\bullet O_2^-$),[1] hydrogen peroxide (H_2O_2),[2] hydroxyl radical ($\bullet OH$),[3] and singlet oxygen ($^1O_2$).[4] In organisms, ROS are generally produced in the mitochondrial electron transport chain and can participate in the regulation of cell signaling pathways to maintain cellular metabolic balance.[5,6] It has been proved that excess ROS, especially oxygen free radicals, can lead to cellular oxidative stress and oxidative damage, which may induce a variety of diseases,[7,8] such as cancer, immune diseases, and neurodegenerative diseases. On the other hand, when mammalian or bacterial cells are exposed to high concentrations of ROS, the cells become more sensitive to oxidative stress, which may further lead to cell death through phospholipid peroxidation, protein oxidation, and DNA damage.[9,10]

With the development of nanobiotechnology and nanomedicine, strategies to utilize excess ROS, generated by nanomaterials under exogenous stimulations (e.g., light, ultrasound [US], microwave, etc.), for disease treatment have attracted extensive attention of researchers and clinicians.[11–13] Among them, photodynamic therapy (PDT), which mainly utilizes photosensitizers and light irradiation to generate ROS, has achieved promising therapeutic effects. However, the application of PDT is limited to superficial tumors due to the low tissue penetration depth of light (~10 mm). Moreover, systemic phototoxicity associated with the retention of photosensitizers is a sore point for PDT.[14] Fortunately, Umemura et al. first discovered that hematoporphyrin induced cancer cell death under US irradiation and named it as sonodynamic therapy (SDT).[15] Further studies revealed that different kinds of molecules and materials as sonosensitizers can react with O_2 to generate excess ROS under US irradiation.[16,17] It should be noted that US is a typical mechanical wave, which can achieve deeper tissue penetration depth (up to ~10 cm) by modulating its frequency. Moreover, US can be focused precisely on the tumor site to achieve targeted activation of sonosensitizers with fewer side effects. The efficacy of SDT depends on the following three basic components: sonosensitizers, tissue oxygen/fluid, and US stimulation.[18] Up to now, the scarcity of highly effective sonosensitizers has limited the development and application of SDT. Inorganic sonosensitizers, which are known for their high stability and low toxicity, are mainly based on semiconductor nanomaterials, such as $PtCu_3$ nanocages, TiO_2 nanoparticles, $MnWO_x$ nanoparticles, etc.[19–21] For these traditional inorganic sonosensitizers, the therapeutic mechanism is ascribed to the energy transfer process caused by sonoluminescence (SL) due to US cavitation effect. The SL phenomenon causes the separation of electrons (e^-) and holes (h^+) in the sonosensitizers, which can further react with oxygen or water molecules to generate cytotoxic ROS. However, due to the inefficient separation and rapid recombination of e^- and h^+, the ROS generation of these inorganic sonosensitizers is still far away from sufficiency.[22,23] Therefore, it is of great significance for improving the SDT efficacy through promoting the separation of e^- and h^+ and inhibiting their rapid recombination in the inorganic sonosensitizers.

Piezoelectric semiconductors (PSs) are a class of materials with both semiconductor and piezoelectric properties, which shows sensitive responsiveness to external stimulations (i.e., light, electric, and force) for modulating separation, transportation, and recombination of charge carriers.[24–28] With these properties, recently, PS and their composite-based nanomaterials have been developed as sonosensitizers to realize highly efficient ROS generation, which paves a new pathway to improve SDT. For PS nanomaterials, even though two underlying mechanisms of ROS generation (energy band theory and screening charge effect) have been proposed, the piezotronic and piezo-phototronic effects on sonodynamic disease therapy have not been fully discussed.[29] This review summarizes the structure and properties of PS and introduces the potential mechanism from the perspective of piezotronic and piezo-phototronic effects, as well as the latest research progress of PS in SDT for cancer treatment and antibacterial applications. Finally, we provide some prospects to the existing problems, challenges, and future development trends in this field.

2 | STRUCTURE OF PS

The piezoelectric effect was discovered by two brothers, Pierre Curie and Jacques Curie, in 1880.[30] When a piezoelectric material is stimulated by an external stress, polarization occurs inside the crystal structure and piezoelectric charges (bound charges) with opposite electrical properties are generated at the opposite ends, which is called the direct piezoelectric effect.[31,32] For a PS, the piezoelectric effect can affect the migration behavior of e^- and h^+ inside the PS, that is the piezotronic effect, which further affects their catalytic performance. Therefore, the structural characteristics of PSs are the basis for understanding the regulation of charge carrier migration behavior via the piezoelectric effect.

2.1 | Asymmetric crystal structure

From the point of view of crystallography, piezoelectric effect is attributed to the asymmetry of the crystal

structure.[33,34] One typical kind of PSs has a perovskite structure with the general chemical formula ABO_3, where A represents lanthanides or alkaline Earth metals and B represents transition metals.[35] Both O and A have a large ionic radius in a cubic close-packed structure, while B locates in the central space of the octahedron due to a small ionic radius,[36] as shown in Figure 1a. As a typical perovskite PS, lead zirconate titanate (PZT) has been widely utilized in the fields of sensing, catalysis, and energy harvesting owing to its excellent piezoelectricity activity and electromechanical coupling coefficient.[38,39] However, the biological toxicity of lead (Pb) in PZT restricts its biomedical applications. Recently, lead-free PSs with perovskite structure have received more attention, such as barium titanate ($BaTiO_3$),[40] bismuth ferrite ($BiFeO_3$),[41] lithium niobate ($LiNbO_3$),[42] potassium sodium niobate (KNN),[43] etc. As a typical biocompatible non-centrosymmetric tetragonal crystal, $BaTiO_3$ shows high piezoelectric activity under external stress owing to the relative displacement of Ti^{4+} in the tetragonal unit cell (Figure 1a).[44]

Another common crystal structure of piezoelectric materials is the wurtzite crystal structure, which belongs to the AB-type hexagonal crystal system with tetrahedral coordination. In this crystal structure, A atoms are distributed in a hexagonal close-packed arrangement, and B atoms occupy tetrahedral voids, such as zinc oxide (ZnO),[45] aluminum nitride (AlN),[46] and gallium nitride (GaN).[47] Taking ZnO as an example, Zn^{2+} and O^{2-} are stacked layer by layer along the *c*-axis in the crystal structure, and the positive and negative charge centers coincide with each other (Figure 1b). Under mechanical stress, the centers of positive and negative charges separate from each other to induce a surface piezoelectric potential, which depends on the applied stress and the doping density of ZnO.[48]

2.2 | Asymmetric stacking structure

From the macroscopic structure, low-dimensional and nanoscale PS materials are more suitable for biomedical applications, such as nanoparticles (NPs), nanowires (NWs), and nanosheets (NSs).[49,50] The ultra-small size not only enables PSs to effectively cross physiological barriers such as blood vessels and cell membranes, but also provides higher carrier migration rate and more active sites for SDT. In addition, low-dimensional PS nanomaterials have higher specific surface areas, which can also be served as drug delivery vehicles.

Notably, some two-dimensional (2D) transition metal dichalcogenides (TMDs) have variable piezoelectric activity depending on the stacking structure. When TMDs such as molybdenum disulfide (MoS_2), tungsten disulfide (WS_2), tin disulfide (SnS_2), tungsten selenide (WSe_2), and tin diselenide ($SnSe_2$) are in the form of stacked bulk materials, they are centrosymmetric and exhibit no piezoelectric activity. On the contrary, when TMDs are thinned to a single layer, the piezoelectric activity appears with the disappearance of the inversion center.[51] Wu et al. first discovered the efficient piezo-catalysis of single- and few-layered MoS_2 nanosheets (MoS_2 NSs), which can rapidly degrade high-concentration organic dyes under US vibration.[52] Another study showed that the piezoelectric activity of MoS_2 NSs weakened with the increase of stacking layers.[37] In addition, MoS_2 with odd-numbered layers is piezoelectrically active, while MoS_2 with even-numbered layers has no piezoelectric activity due to the

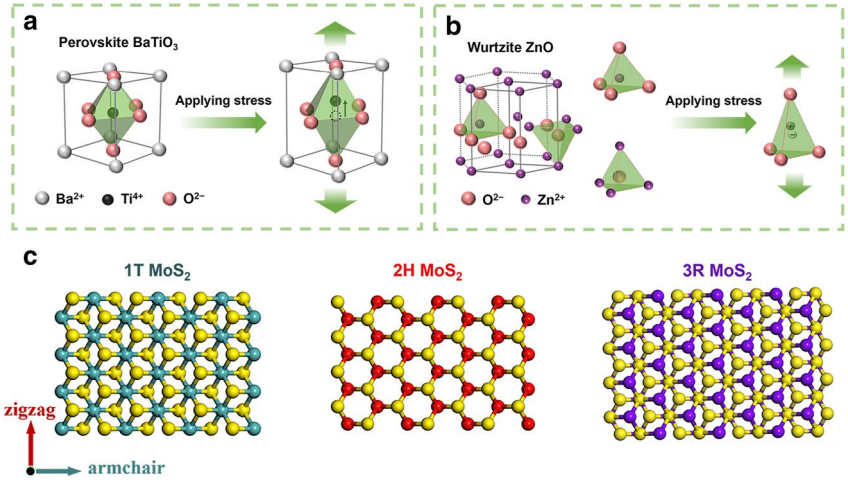

FIGURE 1 Crystal and stacking structure of piezoelectric semiconductors (PSs). (a) Perovskite $BaTiO_3$. (b) Wurtzite ZnO. (c) Schematic diagram of MoS_2 structure of 1T, 2H and 3R phases. (c) Reproduced with permission.[37] Copyright 2021, Elsevier.

asymmetric structure. Moreover, when MoS_2 NSs are arranged in type 3R, the piezoelectric effect accumulates and increases with volume expansion (Figure 1c). Other 2D piezoelectric nanomaterials, including graphene, MXene, transition metal chalcogenides (TMCs), black phosphorus (BP), and hexagonal boron nitride (h-BN), have also been extensively studied theoretically or experimentally.[53]

3 | MECHANISM OF ROS GENERATION IN PSs

Under the stimulation of periodic US, gas molecules and small droplets in the liquid medium can form microbubbles through nucleation and growth, which is called the cavitation effect, as shown in Figure 2a.[54] At present, the mechanism of ROS generation under the cavitation effect is still inconclusive. In this section, we would like to discuss the possible mechanisms of ROS generation from the perspective of PSs.

3.1 | SL and photocatalysis

When the frequencies and intensities of US exceed the threshold, the cavitation effect induces rapid growth and collapse of microbubbles, and finally the energy is released in the form of shock wave and light, also known as SL.[55,56] Therefore, SL-induced photocatalytic reaction is considered as one of the mechanisms of ROS generation in PSs. SL is sub-nanosecond pulsed with wavelengths ranging from 200 to 800 nm, which depends on the properties of the medium and US.[57,58]

According to the energy band theory of semiconductors, when the energy of photons in SL is higher than the forbidden band width ($E \geq E_g$), electrons in PSs can be excited from the valence band (VB) to the conduction band (CB), resulting in the separation of e^- and h^+ (Equation 1). Subsequently, h^+ in the VB and e^- in the CB migrate to the surface of the PS, respectively, and initiate the photocatalytic redox reactions. When the CB edge is more negative than the redox potential of $O_2/\bullet O_2^-$ (−0.33 V vs. RHE), O_2 can be catalyzed to generate $\bullet O_2^-$ (Equation 2).[59] Similarly, when the VB edge is more positive than the redox potential of $H_2O/\bullet OH$ (+2.01 V vs. RHE), it is energetically favorable for the •OH generation from H_2O (Equation 3).[60] Thus, only from the perspective of semiconductor, the band positions of PS for SDT must contain at least one of the $O_2/\bullet O_2^-$ and $H_2O/\bullet OH$ redox potentials to generate free radicals (Figure 2b). Furthermore, the efficiency of photocatalytic reaction is mainly limited by the separation, transportation, and recombination of carriers, so it is vital to regulate the carrier migration behavior for SDT.

$$\text{PS materials} + \text{SL} \rightarrow e^- + h^+, \quad (1)$$

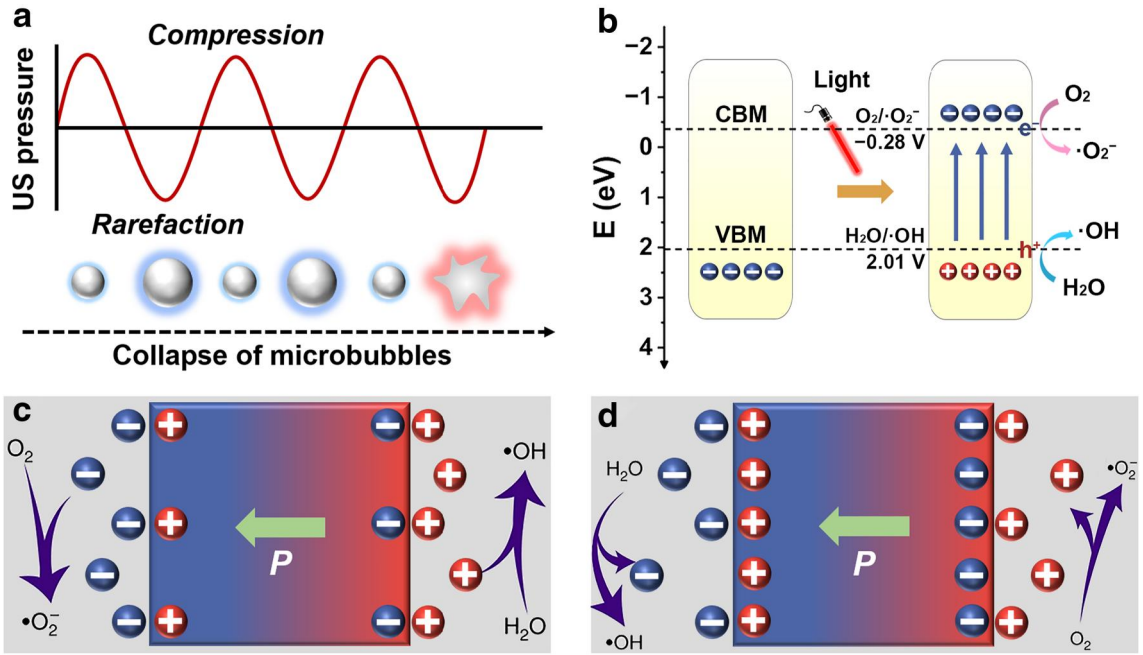

FIGURE 2 Schematic illustration of photocatalysis and piezo-catalysis based on the cavitation effect. (a) Schematic of the cavitation effect under US irradiation. (b) ROS generation during photocatalysis. (c) The release and (d) adsorption of free charges in the solution under compressive stress and then the generation of ROS via piezo-catalysis. ROS, reactive oxygen species; US, ultrasound.

$$e^- + O_2 \rightarrow \bullet O_2^-, \quad (2)$$

$$h^+ + H_2O \rightarrow \bullet OH. \quad (3)$$

In addition, the collapse of microbubbles leads to a local temperature increase, which in turn promotes the separation of e^- and h^+ through thermal excitation and generates oxygen free radicals.[61,62] The process of thermal catalysis is analogous to that of photocatalysis, which will not be repeated here.

3.2 | Piezotronic effect

Taking the theory of photocatalysis and combining with the piezotronic effect, the energy band theory can be partially utilized to explain the ROS generation in PSs. The hypothesis has been proposed that e^- can be directly excited from the VB to the CB by mechanical vibration such as US, and then the reaction with e^- and h^+ produces ROS through a photocatalytic-like pathway.[63] Notably, different from photocatalysis, piezo-catalysis is based on mechanically induced charges rather than photo-induced charges.

Moreover, another mechanism emphasizes the modulation of screening charges by piezotronic effect. In the liquid medium, the bound charge of PS is balanced by the screening charge on the surface of the polarized PS to maintain the overall electrical neutrality. Under the appropriate US intensity, the microbubbles collapse and release ultra-high pressure (up to 10^8 MPa), which is imposed on the PS.[64,65] In the circumstances, the compressive stress based on the piezoelectric effect reduces the polarization of the PS, causing the redistribution of charges and releasing the excess screening charges (Figure 2c); then the excess screening charges are dispersed into the medium and form free charges (Equation 4). Finally, the free charges react with H_2O or/and O_2 in the medium to generate $\bullet OH$ or $\bullet O_2^-$ (Equations 5 and 6).[66]

On the contrary, the polarization of the PS recovers with the decrease of compressive stress, and the PS supplements the screening charges by adsorbing free charges from the medium to balance the bound charges generated by the piezoelectric effect. Meanwhile, the excess charges in the medium continue to trigger the redox reactions and generate ROS (Figure 2d). Therefore, in US vibration and electrolyte environments, PS can continuously provide charges to generate $\bullet OH$ or $\bullet O_2^-$ for SDT.[67] The reaction of piezo-catalysis can be expressed as follows:

$$\text{PS materials} + \text{US} \rightarrow q^- + q^+, \quad (4)$$

$$q^- + O_2 \rightarrow \bullet O_2^-, \quad (5)$$

$$q^+ + H_2O \rightarrow \bullet OH, \quad (6)$$

where q^- and q^+ represent negative charges and positive charges, respectively.

Some other reports considered that mechanical stimulation-induced piezoelectricity can directly trigger the separation of carriers.[68,69] Kubota et al. indicated that mechanical agitation of $BaTiO_3$ can generate a piezoelectric potential (electrochemical potential) for the activation of small organic molecules in organic synthesis.[69] In the borylation, mechanically induced e^- transfer to aryl diazonium salt to furnish aryl radical. The generated radical then reacts with bis(pinacolate) diboron to form the boryl substitution product.

3.3 | Piezo-phototronic effect

In PSs, the coupling of piezoelectric polarization and semiconductor properties also produces a synergistic effect. In 2010, Prof. Wang first proposed the concept of piezo-phototronic effect,[70] which mainly regulates the migration behavior of photo-induced carriers through piezoelectric charges/piezoelectric potentials. It provides a feasible strategy for regulating redox reactions on PS surface.

When the photo-excited PS contacts with the electrolyte solution, the photo-induced carriers migrate into the electrolyte through the solid–liquid interface, which eventually leads to the upward bending of the energy band.[71–73] This type of band bending serves as a barrier for e^- transfer in reduction reactions but can facilitate h^+ transfer in oxidation reactions. If the PS is stimulated by US vibration, the polarized charges generated by the piezoelectric effect spontaneously form an internal electric field.[74,75] Meanwhile, the energy band of the surface with the positively polarized charge bends downward, which means that the US stimulation promotes e^- migration into the electrolyte (reduces the reductive potential) and inhibits h^+ migration (increases the oxidative potential) (Figure 3a, left). Similarly, the energy band of the surface with the negative polarized charge bends upward, leading to further suppression of e^- transfer into the electrolyte (increases the reductive potential) and further promotion of h^+ transfer (reduces the oxidative potential) (Figure 3a, right).[76] Therefore, under the stimulation of US, some PSs that are energetically (in terms of band structure) unfavorable for $\bullet OH$ or $\bullet O_2^-$ generation can produce ROS with the assistance of piezoelectric effect. In addition, based on the piezo-phototronic effect, the construction of

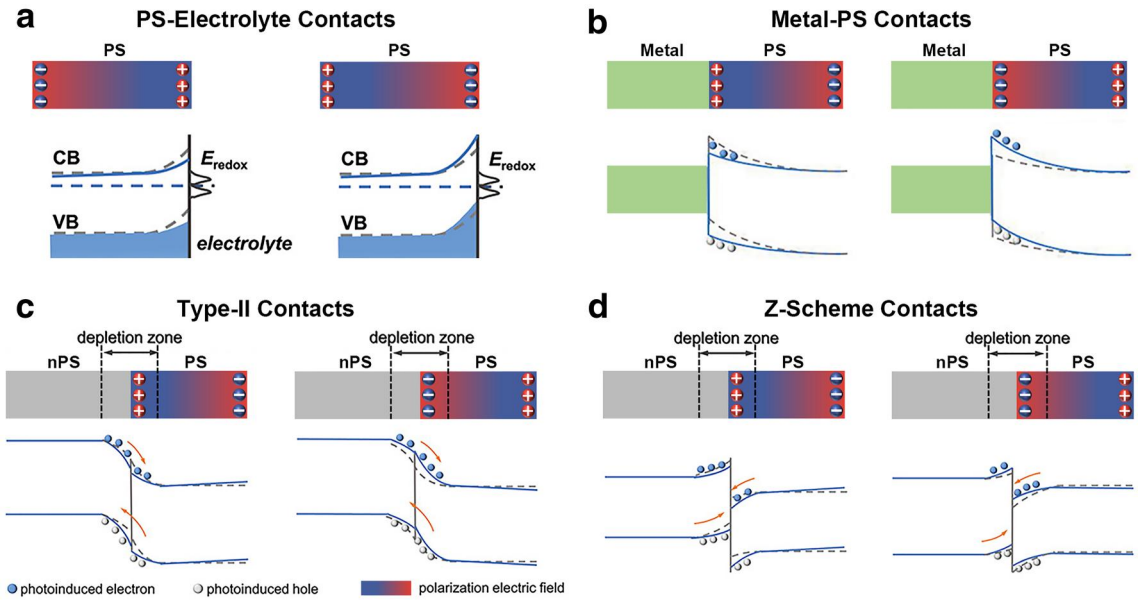

FIGURE 3 Band structure diagrams of the piezoelectric semiconductors (PSs) at the interface. (a) PS-electrolyte contact interface. (b) Metal-PS contact interface. (c) Type-II and (d) Z-scheme contact interfaces.

heterostructures on PSs to regulate the carrier migration behavior has greatly aroused the interest of researchers.

Metal–PS heterojunction

When a PS (with smaller work function) is in contact with a metal (with larger work function), free e^- in the PS migrate to the metal and cause the upward bending of the energy band, forming a Schottky barrier.[77,78] Generally, only photon-induced e^- with energies above the Schottky barrier can cross the heterojunction interface and initiate the reduction reaction. For PSs, the Schottky barrier can be regulated by the mechanically induced piezoelectric potential. If the US vibration induces positive polarization charges at the metal–PS interface, resulting in a lowered Schottky barrier, which is favorable for e^- transfer to promote the reduction reaction (Figure 3b, left). Conversely, when US induces negative polarized charges at the interface, the free electrons are repelled and the Schottky barrier elevates, leading to a decrease in e^- transport to inhibit the reduction reaction (Figure 3b, right).[79]

Type-II and Z-scheme heterojunctions

Furthermore, type-II and Z-scheme heterojunctions have been developed to modulate the migration behavior of charge carriers. The advantages, limitations, and design principles of type-II and Z-scheme heterojunctions are summarized in Table 1. In type-II heterojunction formed from a non-piezoelectric semiconductor (nPS) and a PS, the excited e^- transfers from nPS to PS, while h^+ transfers from PS to nPS, which can remarkably enhance the separation of charge carriers (Figure 3c). Under the US irradiation, the built-in electric field induced by piezoelectric effect takes a decisive role in modulating the migration behavior of the interfacial charges.[80,81] In Figure 3c (left), when the US vibration exerted on PS generates positive polarization charges at the interface, the free electrons are attracted to the depletion region, leading to the downward bending of the energy band and hindering the migration of carriers to the nPS.[82] In contrast, when the negatively polarized charges are introduced at the interface, free electrons are repelled, causing the upward band bending and enhancing the migration to the nPS (Figure 3c, right).

For Z-scheme heterojunction composed of an nPS and a PS, we assume that the nPS has higher band energy level and Fermi level (E_F) than the PS.[83] Once the two semiconductors are in contact with each other, the free electrons at the interface migrate from nPS to PS, and the direction of the electric field at the interface turns from nPS to PS.[84] Under the US excitation, the US-induced h^+ on the nPS recombines with the US-induced e^- on the PS due to the interfacial electric field; while the recombination of e^- on the nPS and h^+ on the PS is inhibited, it preserves the highly reactive e^- and h^+ for efficient catalysis (Figure 3d).[85,86]

Interestingly, a dynamic built-in electric field can be formed inside the PS under US irradiation, which can modulate the migration behavior of e^- and h^+. The positive polarization charges induced by US irradiation leads

TABLE 1 The advantages, limitations, and design principles of type-II and Z-scheme heterojunctions

Categories	Type-II	Z-scheme
Main advantages	• Promote charge separation	• Promote charge separation • Enhance redox ability
Limitations	• Reduce redox ability • Suppress charge transfer	• Induce side reactions • Hard to synthesize
Design principles		
Band alignment	• Staggered ($E_{V1} > E_{V2}$)	• Staggered ($E_{V1} > E_{V2}$)
Fermi level	• $E_{F1} < E_{F2}$	• $E_{F1} > E_{F2}$
Band position	• $E_{V1} > E_O$, $E_{C2} < E_R$	• $E_{V2} > E_O$, $E_{C1} < E_R$

Abbreviations: E_{C1}, CB potential of nPS; E_{C2}, CB potential of PS; E_{F1}, Fermi level of nPS; E_{F2}, Fermi level of PS; E_O, oxidation reaction potential; E_R, reduction reaction potential; E_{V1}, VB potential of nPS; E_{V2}, VB potential of PS.

to the downward band bending of PS, which in turn accelerates the recombination of h^+ on nPS and e^- on PS (Figure 3d, left). In addition, the negatively polarized charges induced by US at the interface suppress the carriers transport in the Z-type heterojunction (Figure 3d, right).[87] Therefore, the construction of PS-based sonosensitizers can effectively improve the transportation of e^- and h^+, further promoting the generation of ROS under US irradiation. Moreover, the US-induced dynamic built-in electric field also modulates the surface redox reactions through band bending, which may enable the redox reactions more energetically favorable for ROS generation.

4 | APPLICATION OF PSs IN SDT

US-mediated SDT has attracted great attention in the biomedical field due to its non-invasive property and deep tissue penetration ability, which is expected to have broader applications than PDT especially for deep-located lesions.[88,89] As a new type of inorganic sonosensitizers, PSs exhibit the advantages of high stability and biocompatibility in vivo, enhanced carrier migration behavior, special physicochemical properties, and easy surface modification for achieving multifunctionalization. Although the research of PS nanomaterials as sonosensitizers for SDT is in its infancy, we believe that this field will become one of the focuses of future research due to their unique carrier migration behavior under US irradiation.

In this section, we focus on the latest research progress of PS nanomaterials as sonosensitizers in SDT and systematically summarize the US parameters (frequency, power, duty cycle, duration, etc.) used for SDT in animal experiments, as shown in Table 2. Up to now, the applications of PS nanomaterials in SDT mainly include cancer therapy and anti-bacteria.

4.1 | Cancer therapy

SDT was originally developed for cancer treatment.[106] In the related studies of PS nanomaterials, researchers found that US irradiation can not only activate PS nanomaterials in deep tumors through cavitation and piezoelectric effects, triggering the generation of cytotoxic ROS but also improve the redox ability of PS nanomaterials through band bending, further promoting ROS generation.

Perovskite nanomaterials

As a kind of classical perovskites nanomaterial, asymmetric tetragonal $BaTiO_3$ nanoparticles (T-BTO NPs) can establish a dynamic built-in electric field under US vibration, by which the separation of e^- and h^+ occurred continuously to trigger redox reactions and produce ROS.[90–92] Inspired by the piezoelectric effect, Zhu et al. prepared T-BTO NPs with a diameter of 106.91 ± 49.72 nm via a typical hydrothermal method, which was used as a new kind of sonosensitizer for cancer SDT.[90] The results of electron spin resonance (ESR) demonstrated that T-BTO aqueous solution showed distinct •OH and $\bullet O_2^-$ characteristic signals under US irradiation, while no significant radical signal was detected in the mere T-BTO or US groups. This may be due to the built-in electric field constructed by the displacement of Ti^{4+} in T-BTO under US stimulation, which can enhance the accumulation of charge carriers on the surface, leading to band bending and initiating •OH and $\bullet O_2^-$ generations. Recently, our group designed and fabricated the $Cu_{2-x}O$-BTO piezoelectric heterostructure as a sonosensitizer for the combination of SDT and chemodynamic therapy (CDT) against cancer (Figure 4a).[91] When $Cu_{2-x}O$-BTO was activated by US stimulation, the polarized piezoelectric

TABLE 2 Various types of PS nanomaterials used in SDT

Applications	Materials	US frequency	US Power	Duty cycle	Duration	Ref.
Cancer therapy	T-BTO	1.0 MHz	1.0 W/cm^2	50%	10 min	[90]
	$Cu_{2-x}O$-BTO	1.0 MHz	1.0 W/cm^2	50%	5 min	[91]
	Bi@BTO	1.0 MHz	1.5 W/cm^2	50%	15 min	[92]
	BP	1.0 MHz	1.5 W/cm^2	/	10 min	[93]
	Bi_2MoO_6	40 kHz	3.0 W/cm^2	50%	5 min	[94]
	FeOCl/FeOOH	1.0 MHz	1.0 W/cm^2	50%	10 min	[95]
	Au@BP	1.0 MHz	2.0 W/cm^2	40%	2.5 min	[96]
	D-ZnO_x:Gd	1.0 MHz	1.0 W/cm^2	50%	/	[97]
	Au@P-ZnO	1.0 MHz	0.5 W/cm^2	50%	2 min	[98]
	HA@$MoCF_3Pt$	1.0 MHz	1.0 W/cm^2	/	15 min	[99]
	NSH700	0.8 MHz	0.5 W/cm^2	50%	10 min	[100]
Anti-bacteria	S-BTO	1.0 MHz	1.5 W/cm^2 1.0 W/cm^2	50%	20 min 5 min	[101]
	Au@BTO	1.0 MHz	1.5 W/cm^2	50%	3 min	[102]
	ZnO-GO	24 kHz	40 W	/	10 min	[103]
	ZnO@GDY	1.0 MHz	1.0 W/cm^2	50%	30 min	[104]
	HNTM-MoS_2	1.0 MHz	1.5 W/cm^2	50%	15 min	[105]

Note: "/" means not given in the publications.

Abbreviations: SDT, sonodynamic therapy; US, ultrasound.

field promoted the migration of US-induced charge carriers (e^- and h^+), further causing the band bending that shifted the CB and VB to better positions for triggering the generation of •OH and $•O_2^-$. Furthermore, owing to the existence of Cu(I) in the heterojunction, $Cu_{2-x}O$-BTO showed excellent Fenton-like activity to generate •OH from endogenous H_2O_2 in a tumor microenvironment (TME), enabling CDT to directly induce cancer cell apoptosis.[107] The in vivo experiments also demonstrated that the combination of SDT and CDT achieved potent tumor inhibition in 4T1 tumor-bearing mice (Figure 4b). It is noteworthy that the CDT efficacy can be further promoted with the assistance of US through electron lever strategy due to the increased electron density of the active sites in the piezoelectric perovskite nanocrystals.[108]

2D-layered nanomaterials

Few-layer black phosphorus nanosheets (BP NSs) are typical 2D semiconductors with piezoelectric activity, which displayed significant ROS generation under US irradiation.[109,110] Li et al. prepared few-layer BP NSs through liquid-phase exfoliation and investigated the US-induced cytotoxicity as well as in vivo antitumor activity (Figure 4c).[93] The intrinsic bandgap of BP NSs was measured to be 0.84 V, with the CB and VB edges of −0.39 and 0.45 V versus RHE, respectively. The CB edge was more negative than the redox potential of $O_2/•O_2^-$ indicating that the e^- on CB was energetically favorable for the $•O_2^-$ generation. In addition, when BP NSs were exposed to US stimulation, the built-in electric field formed by the piezoelectric effect resulted in band bending, making the VB position more positive than the redox potential of H_2O/•OH to initiate the •OH production (Figure 4d). To detect the species of ROS, 9,10-anthracenediyl-bis(methylene)-dimalonic acid (ABDA) and terephthalic acid (TA) were selected as specific probes of $^1O_2$ and •OH, respectively.[111] As a result, the ROS generated by BP NSs under US irradiation was mainly •OH rather than $^1O_2$. The detection of intracellular ROS stained with 2′,7′-dichlorodihydrofluorescein diacetate (DCFH-DA) showed a partial oxygen-dependent ROS-production under US stimulation, which may provide a solution to overcome the hypoxia features of TME. Besides BP NSs, WS_2, and MoS_2 NSs with piezoelectric activity also have the potential to be used as sonosensitizers for SDT.[112]

High level of glutathione (GSH, 1–10 mM) is one of the main characteristics of TME, which renders cancer cells resistant to oxidative stress, thereby weakening the efficacy of SDT.[113] Depletion of GSH is used as an

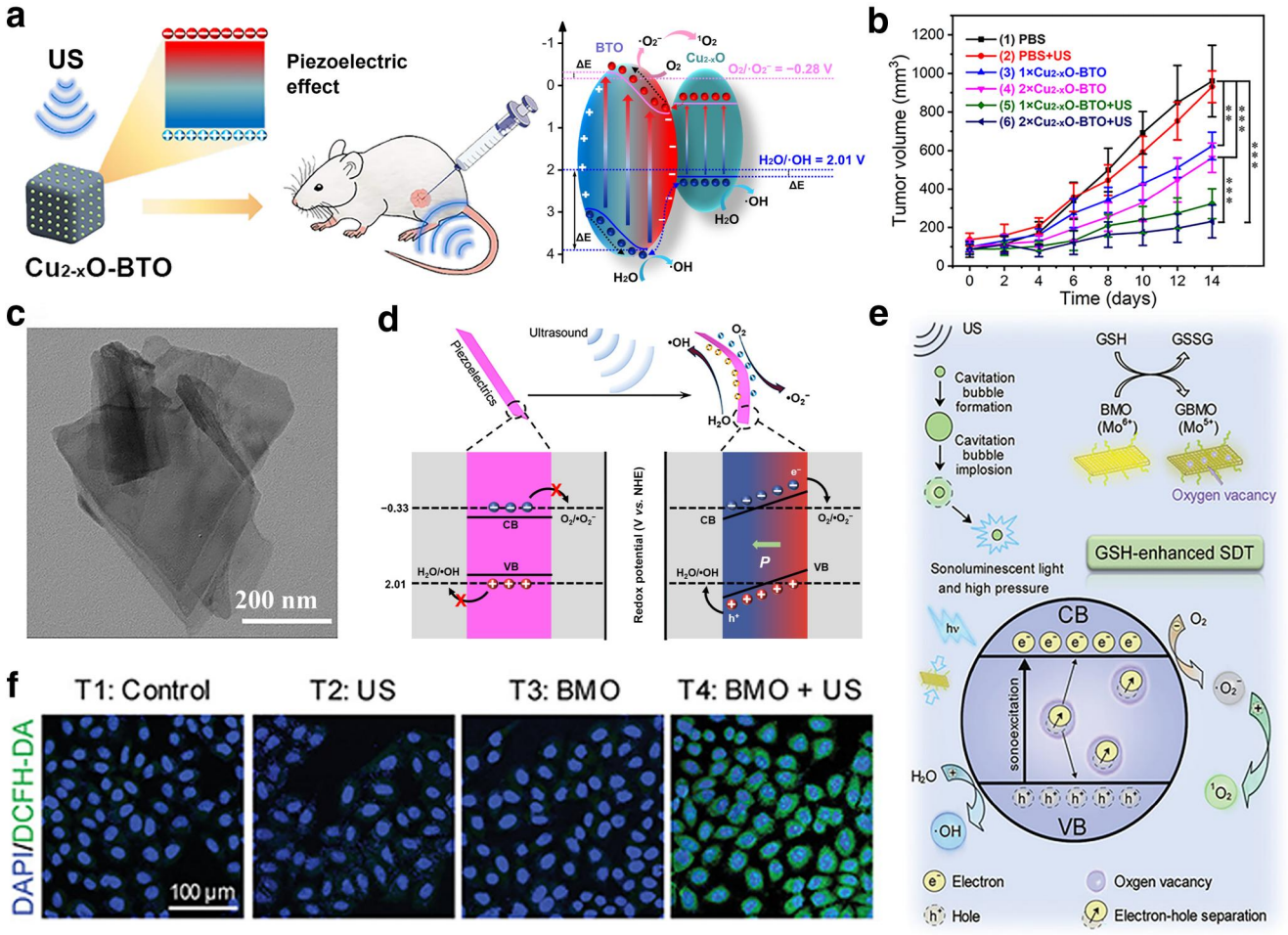

FIGURE 4 Applications of PS nanomaterials in SDT of cancer. (a) Schematic illustration of cancer SDT and band tilting of $Cu_{2-x}O$-BTO. (b) Tumor growth curves after different treatments. (***p<0.001, **p<0.01) (c) TEM image and (d) schematic illustration on energy band of BP nanosheet. (e) Mechanism of BMO for GSH-enhanced SDT, and (f) intracellular ROS level of HeLa cells after different treatments. (b) Reproduced with permission.[91] Copyright 2022, American Chemical Society. (c) Reproduced with permission.[93] Copyright 2020, American Chemical Society. (e, f) Reproduced with permission.[94] Copyright 2021, Wiley-VCH. BP, black phosphorus; GSH, glutathione; PS, piezoelectric semiconductor; ROS, reactive oxygen species; SDT, sonodynamic therapy.

auxiliary pathway to improve cancer therapy, and GSH can also act as an endogenous trigger to enhance cancer therapy. Dong et al. presented a successful paradigm of employing a PS sonosensitizer for endogenous GSH-enhanced SDT (Figure 4e).[94] Specifically, bismuth molybdate (Bi_2MoO_6) with 2D piezoelectric structure was synthesized via a hydrothermal process. After modification with poly(ethylene glycol) (PEG), the obtained Bi_2MoO_6 nanoribbons (BMO NRs) exhibited good biocompatibility and physiological stability and displayed US-induced generation of $^1O_2$ and •OH. In addition, BMO NRs showed an excellent GSH depletion ability through a redox reaction with GSH to generate Mo^{5+} and oxygen vacancies. Significantly, the GSH-activated BMO showed an enhanced sonodynamic performance compared with BMO NR. Under US irradiation, the built-in electric field of BMO NRs promoted the migration of e^- and h^+ to opposite sides, resulting in band bending and reducing the distance between the band edges and the redox potentials of $O_2/•O_2^-$ and $H_2O/•OH$. Meanwhile, the oxygen vacancies on the surface of BMO NRs effectively inhibited the recombination of e^- and h^+, thereby enhancing the yield of ROS in SDT (Figure 4f). In vivo SDT results proved that BMO NRs not only exhibited satisfactory biocompatibility, but also effectively suppressed tumor growth.

Construction of heterojunctions and defects

From the macroscopic aspect, one-dimensional (1D) or 2D PSs are more likely to generate large elastic deformation and high piezoelectric potential under only a tiny mechanical force, which is conducive to the regulation

of energy band structure and carrier migration behavior.[95,114] Therefore, 1D and 2D PS nanomaterials, with most atoms exposed on the surface, are ideal candidates for SDT. In addition, researchers have improved the efficacy of SDT through constructing heterojunctions or introducing defects on piezoelectric PS nanomaterials. Ouyang et al. successfully synthesized a 2D PS sonosensitizer (Au@BP nanohybrid) by in situ growth of Au NPs on BP NSs under US stimulation, which was used for efficient $^1O_2$ generation in SDT (Figure 5a).[96] During the formation of the Au@BP nanohybrid, the BP NSs have dual roles, which can be used not only as a reductant for the formation of Au NPs, but also as a nanostabilizer for the assembly of Au NPs on the surface of BP. When using singlet oxygen sensor green (SOSG) as the probe to detect $^1O_2$ generation of BP and Au@BP, Au@BP nanohybrid showed much stronger $^1O_2$ generation ability than BP NSs (~5-folds) under US irradiation (Figure 5b). When Au@BP was exposed to US, e^- were excited from the VB to CB, leaving h^+ on the VB. Due to the Fermi level of BP (−3.9 eV) being higher than that of Au (−5.1 eV), e^- can be transferred from BP to Au, forming Schottky contact.[115,116] The Schottky barrier can effectively inhibit the recombination of e^- and h^+, which in turn promoted the transfer of e^- to the surrounding oxygen molecules to generate $^1O_2$. Both in vitro and in vivo experiments demonstrated that Au@BP nanohybrid significantly killed tumor cells and inhibited tumor growth under US irradiation with less side effects.

In another study, Liu et al. attempted to improve the sonodynamic performance of PS sonosensitizers through a defect engineering strategy (Figure 5c).[97] The defect-rich gadolinium (Gd)-doped zinc oxide nanobullet (D-ZnO_x:Gd) was successfully synthesized by inert gas deoxidation method for magnetic resonance imaging (MRI)-guided

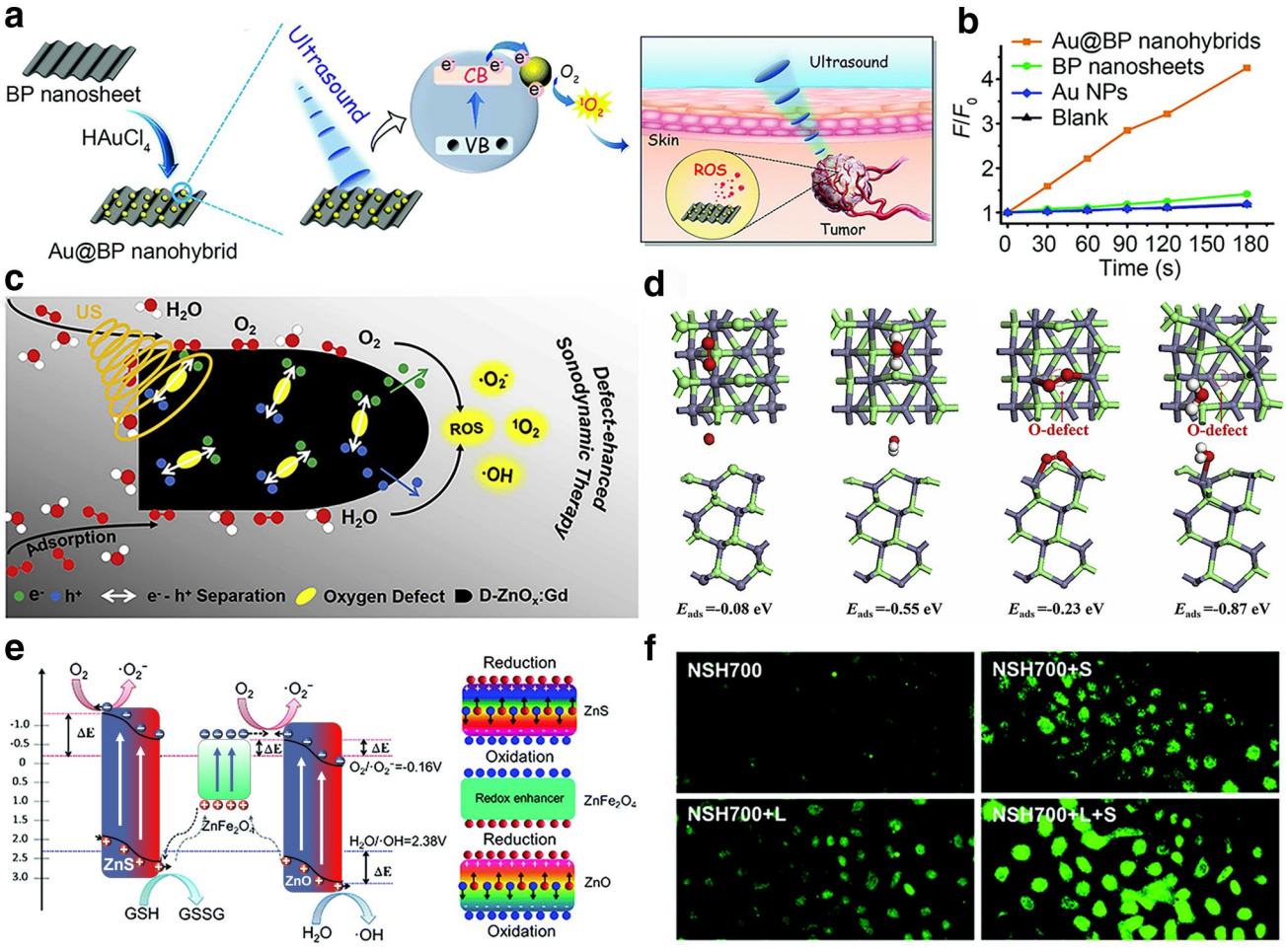

FIGURE 5 Application of PS heterojunctions in cancer SDT. (a) Schematic illustration of Au@BP nanohybrid in cancer SDT, and (b) fluorescence of SOSG under US. (c) Mechanism for enhanced ROS generation by D-ZnO_x:Gd. (d) Adsorption energies of O_2 and H_2O on ZnO and D-ZnO_x:Gd, respectively. (e) Schematic diagram of carriers transport behavior in NSH700, and (f) intracellular ROS generation. (a, b) Reproduced with permission.[96] Copyright 2018, Royal Society of Chemistry. (c, d) Reproduced with permission.[97] Copyright 2020, Elsevier. (f) Reproduced with permission.[100] Copyright 2021, Royal Society of Chemistry. PS, piezoelectric semiconductor; ROS, reactive oxygen species; SDT, sonodynamic therapy; SOSG, singlet oxygen sensor green; US, ultrasound.

SDT. Then, dihydroethidium, SOSG, and hydroxyphenyl fluorescein (HPF) were used to prove that the generated ROS mainly included $\bullet O_2^-$, $^1O_2$, and •OH.[98,99] Compared with defect-free ZnO and defect-free ZnO:Gd, D-ZnO_x:Gd exhibited better ROS production ability under US irradiation, which was attributed to the existence of defects that promoted the transportation and separation of charge carriers. Moreover, the adsorption energies of O_2 and H_2O on the D-ZnO_x:Gd surface were enhanced by 0.15 and 0.32 eV (Figure 5d), respectively, which would further promote the generation of ROS. Due to the doping of Gd, D-ZnOx:Gd could act as a T_1-weighted MRI contrast, and D-ZnO_x:Gd mediated SDT can effectively inhibit tumor growth in vivo under the guidance of MRI. Similarly, Kang et al. integrated the photocatalytic properties with piezoelectric polarization into single natural sphalerite (NSH) nanosheets via calcination and exfoliation strategy.[100] The NSH composed of ZnS and FeS was turned into ZnS/$ZnFe_2O_4$/ZnO (NSH700) after calcination at 700°C, which exhibited efficient catalytic performance through the piezo-phototronic effect in this heterojunction. In Figure 5e, the as-prepared NSH700 can maximally suppress the recombination of electrons and holes, resulting in ROS burst. Under light and US irradiation, a built-in electric field was constructed in piezoelectric ZnO and ZnS, which improved the separation of carriers in $ZnFe_2O_4$ and guided the migration of carriers to the surface. Moreover, as exhibited in Figure 5f, the cancer cells treated with NSH700 NSs showed the highest ROS generation under both light and US irradiation. In vivo experiments on MCF-7 tumor-bearing mice showed that under light and US stimulation, the designed NSH700 NSs can significantly inhibit tumor growth.

These progresses demonstrated that PS nanomaterials exhibited great potential as sonosensitizers in cancer SDT. In addition, rationally designing defects or heterostructures on PSs can further facilitate the separation and transportation of carriers, thereby enhancing the efficacy of SDT. Importantly, the construction of oxygen vacancies not only facilitates ROS generation but also exhibits additional properties such as enzyme-like activity for improving ROS generation and therapy. Furthermore, considering the characteristics of tumor TME of acidic pH, hypoxia, high levels of H_2O_2, and GSH, designing PS sonosensitizers with TME responsiveness is also a potential way to improve the efficacy of SDT.

4.2 | Anti-bacteria

The clinical method for treating bacterial infections requires high-dose and long-term systemic antibiotics administration, which may lead to systemic toxicity and antibiotic resistance.[117,118] Therefore, it is highly desirable to develop antibiotic-free therapeutic strategies for bacterial infections. As an emerging technology, SDT also shows unique potential in anti-bacteria and treatment of infectious diseases. Under US stimulation, PS nanomaterials can catalyze the production of highly cytotoxic ROS to kill bacteria without worrying about drug resistance.[119]

In 2018, our group fabricated 1D piezoelectric TiO_2-$BaTiO_3$-Au heterojunction for antibacterial application under light irradiation via piezo-phototronic effect, which opens the passage for using PS nanomaterials in this field.[26] In this work, the remnant polarization in $BaTiO_3$ was induced by positive polarization, and the dynamic built-in electric field was stimulated by light irradiation rather than US irradiation. Soon after, Masimukku et al. synthesized tungsten disulfide nanoflowers (WS_2 NFs) with piezoelectric activity via a hydrothermal method and demonstrated their sonodynamic antibacterial properties for the first time (Figure 6a).[120] Under the US irradiation, WS_2 NFs were polarized, which promoted the migration of e^- and h^+ to the surface in opposite directions and catalyzed the generation of ROS. Further ESR characterization demonstrated that the ROS generated by WS_2 NFs under US stimulation were mainly $^1O_2$ and •OH. In vitro antibacterial experiments showed that the antibacterial properties of single- and few-layer WS_2 NFs against *Escherichia coli* reached over 99.99% within 60 min under US stimulation (Figure 6b).

To further improve the electron-hole separation of PS sonosensitizers in SDT,[101] our group constructed the $BaTiO_3$ sonosensitizer loaded with Au NPs (Au@BTO) for SDT of wound infection in mice.[102] As shown in Figure 6c, the as-prepared Au@BTO had a Schottky heterojunction structure, which can promote the separation of e^- and h^+ and enhance the SDT efficacy under the action of US. The in vitro experiment showed that after US irradiation for 4 min, the antibacterial efficiencies of Au@BTO against *E. coli* and *Staphylococcus aureus* reached 99.23% and 99.94%, respectively (Figure 6d). Au@BTO also showed excellent antibacterial effect in a mouse model with a *S. aureus*-infected wound. Interestingly, it was found that the ROS generated during SDT not only had significant antibacterial activity but also promoted cell proliferation and migration of fibroblasts and macrophages, which can significantly accelerate wound healing (Figure 6e,f). This study broadens the application of PS nanomaterials as sonosensitizers in antibacterial SDT applications. Besides perovskite structured PS, ZnO with wurtzite structure has also been developed for antibacterial SDT based on piezoelectric effect and has shown an excellent antibacterial effect both in vitro and in vivo.[103,104]

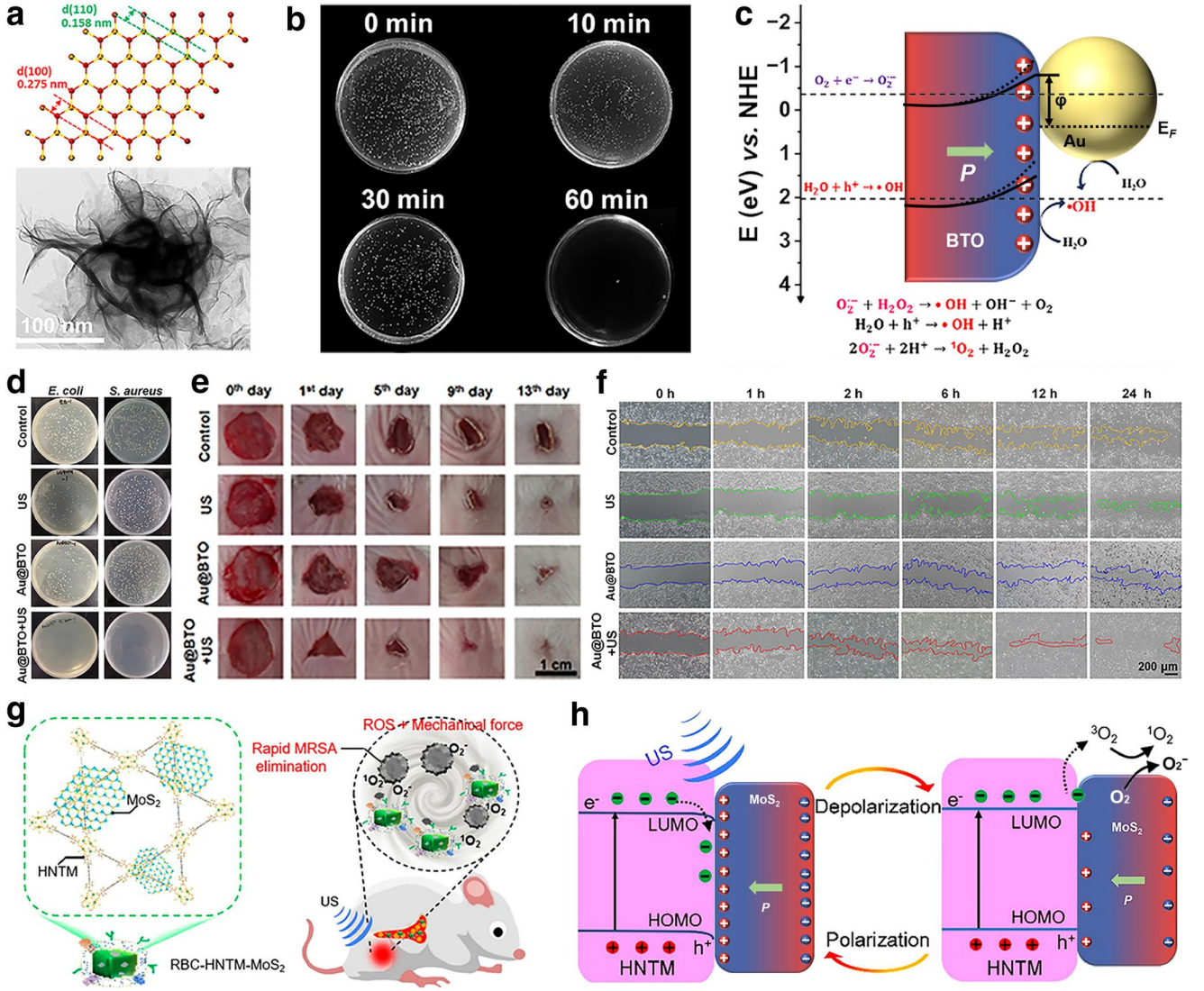

FIGURE 6 Application of PS nanomaterials in antibacterial SDT. (a) TEM image and atomic structure of WS_2 NFs. (b) Antibacterial SDT of WS_2 NFs against *Escherichia coli*. (c) Mechanism of Au@BTO in antibacterial SDT. (d) Antibacterial SDT of Au@BTO against *E. coli* and *Staphylococcus aureus*. (e) Photographs of the infected wounds during therapy. (f) Images of NIH-3T3 cell migration. (g) Schematic diagram and (h) mechanism of HNTM-MoS_2 in antibacterial SDT. (a, b) Reproduced with permission.[120] Copyright 2018, Elsevier. (d–f) Reproduced with permission.[102] Copyright 2021, Elsevier. (g) Reproduced with permission.[105] Copyright 2022, American Chemical Society. PS, piezoelectric semiconductor; SDT, sonodynamic therapy.

Significantly, due to the noninvasiveness and high tissue penetration of US, SDT has a lower risk of systemic toxic side-effects and shows great potential in the treatment of deep infection. Feng et al. prepared a piezoelectric-enhanced sonosensitizer for SDT of osteomyelitis in vivo.[105] MoS_2 NSs with piezoelectric activity were surface-modified with porphyrin-based hollow metal-organic framework (HNTM) through electrostatic interactions (Figure 6g). Different from the material designs mentioned above, the non-piezoelectric HNTM in HNTM-MoS_2 heterojunction was used as a sonosensitizer, while MoS_2 NSs with piezoelectric effect were chosen to augment the charge transport at the heterogeneous interface through the US-induced piezoelectric polarization (Figure 6h). In addition, the detection of ROS with 9,10-dimethylanthracene (DMA, $^1O_2$ probe), nitro blue tetrazolium (NBT, $\cdot O_2^-$ probe), and TA ($\cdot$OH probe) indicated that the types of ROS generated under US treatment were mainly $^1O_2$ and $\cdot O_2^-$, rather than $\cdot$OH.[121] Comparably, HNTM-MoS_2 showed stronger ROS generation capacity than HNTM under US irradiation, which predicted better SDT efficacy. Both in vitro and in vivo experiments demonstrated that the formation of HNTM-MoS_2 heterojunctions not only enhanced the antibacterial SDT ability, killed methicillin-resistant *S. aureus* in the bone marrow, and eliminated bone infection but also

inhibited inflammation and bone loss. This study provides another strategy for the use of PSs in the antibacterial SDT of deep infections.

In general, benefiting from the deep tissue penetration of US, SDT with PS nanomaterials as sonosensitizers can be used not only for superficial wound bacterial infections but also for deep bacterial infections. In addition, the construction of heterojunction can promote the separation and transportation of US-induced charge carriers, thereby enhancing the generation of ROS and the efficacy of SDT.

5 | CHALLENGES AND PROSPECTS

SDT, as a new type of non-invasive treatment strategy, is gradually attracting attention. However, the lack of efficient sonosensitizers has seriously hindered further development of SDT. With regard to stable and biocompatible inorganic sonosensitizers, the rapid recombination of charge carriers is one of the most leading causes for low SDT efficiency. Starting from the structure of PSs, this paper summarizes the potential mechanisms of the new-rising PSs as sonosensitizers for SDT: (1) SL and photocatalysis; (2) piezo-catalysis; and (3) piezo-phototronic effect. In addition, the related research progress of PSs for SDT for several years is reviewed, mainly including the applications in cancer therapy and anti-bacteria.

Although PS nanomaterials as sonosensitizers have made initial progress in the field of SDT, there are still some challenges that require further research studies, which are summarized as follows: (1) Many PSs contain heavy metal elements (Cd, Pb, Co, etc.), thus requiring comprehensive toxicity assessment to ensure biosafety. If needed, surface modification might reduce the possible toxicity of the PSs. (2) Nanomaterials and heterostructures with enhanced piezoelectricity and charge carrier transport behavior are required to further improve SDT efficacy. (3) Mass-production synthetic techniques for size-controllable PS nanomaterials are needed, which is the pre-condition for possible translation. (4) Inappropriate US irradiation might generate uncertainty and damage to cells; it is required to study the interaction between PSs and US conditions, thus precisely matching the US condition (frequency, power, duty cycle, duration, etc.) and TME with the PSs to realize an optimal SDT efficacy. (5) To improve bioavailability, researchers should control the appropriate structure and particle size, investigate metabolic pathways, optimize administration routes, or tether targeting ligands to the PSs for improving their targeting and accumulation in lesion locations. In addition, the SDT mechanism of PS sonosensitizers also remains ambiguous and needs to be elucidated.

Regarding the materials design with enhanced piezoelectricity and charge carrier migration behavior, the choice of PS nanomaterial is paramount. The energy band position of the selected PS nanomaterials should be as close as possible to the redox potentials of $O_2/\bullet O_2^-$ and $H_2O/\bullet OH$, so that a small band bending under US can also promote ROS generation. Notably, apart from ROS generation, other cytotoxic free radicals (e.g., sulfate, nitroxide, and alkoxyl radicals) can be generated by PSs under US irradiation, which also provides a possible future direction of sonosensitizer design.[122] Second, the asymmetry of the crystal structure in PSs can be increased by element doping, thereby enhancing the piezoelectric responsiveness. Third, it is efficient to introduce atom defects (e.g., oxygen vacancy) to form electron potential wells for suppressing the recombination of electrons and holes. Finally, heterojunctions can be constructed to promote the separation and transportation of electrons and holes and prevent rapid recombination. Furthermore, synergistic therapies through combining SDT with other strategies, such as chemotherapy, immunotherapy, gas therapy, photothermal therapy (PTT), PDT, and CDT, can also improve the final therapeutic outcome.[123–125]

In conclusion, future related research is not only of great significance to expand the functional application of PS nanomaterials but also has potential value for the development and clinical translation of SDT.

ACKNOWLEDGMENTS

This work was supported by the National Natural Science Foundation of China (No. 82072065, 81471784), the Strategic Priority Research Program of the Chinese Academy of Sciences (No. XDA16021103), the Fundamental Research Funds for the Central Universities (E2EG6802X2), and the National Youth Talent Support Program.

CONFLICT OF INTEREST

The authors declare no conflict of interest.

ORCID

Linlin Li https://orcid.org/0000-0003-1041-4533

REFERENCES

1. M. Hayyan, M. A. Hashim, I. M. AlNashef, *Chem. Rev.* **2016**, *116*, 3029.
2. G. Bodega, M. Alique, L. Puebla, J. Carracedo, R. M. Ramírez, *J. Extracell. Vesicles* **2019**, *8*, 1626654.
3. S. Gligorovski, R. Strekowski, S. Barbati, D. Vione, *Chem. Rev.* **2015**, *115*, 13051.
4. S. Yao, Z. Wang, L. Li, *Smart Mater. Med.* **2022**, *3*, 230.
5. Y. Yao, H. Zhang, Z. Wang, J. Ding, S. Wang, B. Huang, S. Kea, C. Gao, *J. Mater. Chem. B* **2019**, *7*, 5019.
6. R. Alhayaza, E. Haque, C. Karbasiafshar, F. W. Sellke, M. R. Abid, *Front. Chem.* **2020**, *8*, 592688.

7. Z. Cao, D. Li, J. Wang, X. Yang, *Acta Biomater.* **2021**, *130*, 17.
8. S. Yao, Z. Liu, L. Li, *Nano-Micro Lett.* **2021**, *13*, 176.
9. Y. He, S. H. Liu, J. Yin, J. Yoon, *Coord. Chem. Rev.* **2021**, *429*, 213610.
10. Y. S. Bae, H. Oh, S. G. Rhee, Y. D. Yoo, *Mol. Cells* **2011**, *32*, 491.
11. M. Wu, Y. Ding, L. Li, *Nanoscale* **2019**, *11*, 19658.
12. S. Yao, X. Zhao, X. Wan, X. Wang, T. Huang, J. Zhang, L. Li, *Mater. Horiz.* **2021**, *8*, 3457.
13. B. Ma, S. Wang, F. Liu, S. Zhang, J. Duan, Z. Li, Y. Kong, Y. Sang, H. Liu, W. Bu, L. Li, *J. Am. Chem. Soc.* **2019**, *141*, 849.
14. X. Zhao, S. Yao, X. Wan, T. Huang, Z. Zhang, X. Wang, S. Wang, Q. Liang, Z. Li, L. Li, *Appl. Mater. Today* **2021**, *25*, 101255.
15. N. Yumita, R. Nishigaki, K. Umemura, S. Umemura, *Jpn. J. Cancer Res.* **1989**, *80*, 219.
16. R. Liu, Q. Zhang, Y. Lang, Z. Peng, L. Li, *Photodiagn. Photodyn. Ther.* **2017**, *19*, 159.
17. X. Lin, Y. Qiu, L. Song, S. Chen, X. Chen, G. Huang, J. Song, X. Chen, H. Yang, *Nanoscale Horiz.* **2019**, *4*, 747.
18. J. Chen, H. Luo, Y. Liu, W. Zhang, H. Li, T. Luo, K. Zhang, Y. Zhao, J. Liu, *ACS Nano* **2017**, *11*, 12849.
19. V. G. Deepagan, D. G. You, W. Um, H. Ko, S. Kwon, K. Y. Choi, G. R. Yi, J. Y. Lee, D. S. Lee, K. Kim, I. C. Kwon, J. H. Park, *Nano Lett.* **2016**, *16*, 6257.
20. F. Gong, L. Cheng, N. Yang, O. Betzer, L. Feng, Q. Zhou, Y. Li, R. Chen, R. Popovtzer, Z. Liu, *Adv. Mater.* **2019**, *31*, 1900730.
21. X. Zhong, X. Wang, L. Cheng, Y. Tang, G. Zhan, F. Gong, R. Zhang, J. Hu, Z. Liu, X. Yang, *Adv. Funct. Mater.* **2020**, *30*, 1907954.
22. H. Zhang, X. Pan, Q. Wu, J. Guo, C. Wang, H. Liu, *Exploration* **2021**, *1*, 20210010.
23. X. Han, J. Huang, X. Jing, D. Yang, H. Lin, Z. Wang, P. Li, Y. Chen, *ACS Nano* **2018**, *12*, 4545.
24. D. Xiang, Z. Liu, M. Wu, H. Liu, X. Zhang, Z. Wang, Z. L. Wang, L. Li, *Small* **2020**, *16*, 1907603.
25. Z. Liu, L. Wang, X. Yu, J. Zhang, R. Yang, X. Zhang, Y. Ji, M. Wu, L. Deng, L. Li, Z. L. Wang, *Adv. Funct. Mater.* **2019**, *29*, 1807279.
26. X. Yu, S. Wang, X. Zhang, A. Qi, X. Qiao, Z. Liu, M. Wu, L. Li, Z. L. Wang, *Nano Energy* **2018**, *46*, 29.
27. W. Wu, Z. L. Wang, *Nat. Rev. Mater.* **2016**, *1*, 16031.
28. X. Wan, X. Zhang, Z. Liu, J. Zhang, Z. Li, Z. L. Wang, L. Li, *Appl. Mater. Today* **2021**, *25*, 101218.
29. S. Tu, Y. Guo, Y. Zhang, C. Hu, T. Zhang, T. Ma, H. Huang, *Adv. Funct. Mater.* **2020**, *30*, 2005158.
30. J. Curie, P. Curie, *Bull. Mineral.* **1880**, *3*, 90.
31. M. T. Chorsi, E. J. Curry, H. T. Chorsi, R. Das, J. Baroody, P. K. Purohit, H. Ilies, T. D. Nguyen, *Adv. Mater.* **2019**, *31*, 1802084.
32. C. Wan, C. R. Bowen, *J. Mater. Chem.* **2017**, *5*, 3091.
33. Z. Wang, Z. Liu, G. Zhao, Z. Zhang, X. Zhao, X. Wan, Y. Zhang, Z. L. Wang, L. Li, *ACS Nano* **2022**, *16*, 1661.
34. Q. Xu, X. Gao, S. Zhao, Y. N. Liu, D. Zhang, K. Zhou, H. Khanbareh, W. Chen, Y. Zhang, C. Bowen, *Adv. Mater.* **2021**, *33*, 2008452.
35. W. Wang, M. Xu, X. Xu, W. Zhou, Z. Shao, *Angew. Chem., Int. Ed.* **2020**, *59*, 136.
36. X. Li, H. Zhao, J. Liang, Y. Luo, G. Chen, X. Shi, S. Lu, S. Gao, J. Hu, Q. Liu, X. Sun, *J. Mater. Chem.* **2021**, *9*, 6650.
37. T. Ren, W. Tian, Q. Shen, Z. Yuan, D. Chen, N. Li, J. Lu, *Nano Energy* **2021**, *90*, 106527.
38. Y. Zang, F. Zhang, C. Di, D. Zhu, *Mater. Horiz.* **2015**, *2*, 140.
39. S. Priya, H. C. Song, Y. Zhou, R. Varghese, A. Chopra, S. G. Kim, I. Kanno, L. Wu, D. S. Ha, J. Ryu, R. G. Polcawich, *Energy Harvest. Syst.* **2017**, *4*, 3.
40. C. K. Jeong, I. Kim, K. I. Park, M. H. Oh, H. Paik, G. T. Hwang, K. No, Y. S. Nam, K. J. Lee, *ACS Nano* **2013**, *7*, 11016.
41. L. Fei, Y. Hu, X. Li, R. Song, L. Sun, H. Huang, H. Gu, H. L. W. Chan, Y. Wang, *ACS Appl. Mater. Interfaces* **2015**, *7*, 3665.
42. Y. Wang, X. Y. Zhou, Z. Chen, B. Cai, Z. Z. Ye, C. Y. Gao, J. Y. Huang, *Appl. Phys. A.* **2014**, *117*, 2121.
43. S. W. Yu, S. T. Kuo, W. H. Tuan, Y. Y. Tsai, S. F. Wang, *Ceram. Int.* **2012**, *38*, 2845.
44. H. Wei, H. Wang, Y. Xia, D. Cui, Y. Shi, M. Dong, C. Liu, T. Ding, J. Zhang, Y. Ma, N. Wang, Z. Wang, Y. Sun, R. Wei, Z. Guo, *J. Mater. Chem. C* **2018**, *6*, 12446.
45. C. Dagdeviren, S. W. Hwang, Y. Su, S. Kim, H. Cheng, O. Gur, R. Haney, F. G. Omenetto, Y. Huang, J. A. Rogers, *Small* **2013**, *9*, 3398.
46. N. Jackson, L. Keeney, A. Mathewson, *Smart Mater. Struct.* **2013**, *22*, 115033.
47. S. A. Jewett, M. S. Makowski, B. Andrews, M. J. Manfra, A. Ivanisevic, *Acta Biomater.* **2012**, *8*, 728.
48. R. K. Pandey, J. Dutta, S. Brahma, B. Rao, C. P. Liu, *J. Phys. Mater.* **2021**, *4*, 044011.
49. M. Aflori, *Nanomaterials* **2021**, *11*, 396.
50. S. M. George, B. Kandasubramanian, *Ceram. Int.* **2020**, *46*, 8522.
51. R. Hinchet, U. Khan, C. Falconi, S. W. Kim, *Mater. Today* **2018**, *21*, 611.
52. J. M. Wu, W. E. Chang, Y. T. Chang, C. K. Chang, *Adv. Mater.* **2016**, *28*, 3718.
53. P. C. Sherrell, M. Fronzi, N. A. Shepelin, A. Corletto, D. A. Winkler, M. Ford, J. G. Shapter, A. V. Ellis, *Chem. Soc. Rev.* **2022**, *51*, 650.
54. W. Um, E. K. P. Kumar, J. Lee, C. H. Kim, D. G. You, J. H. Park, *Chem. Commun.* **2021**, *57*, 2854.
55. H. Xu, K. S. Suslick, *Phys. Rev. Lett.* **2010**, *104*, 244301.
56. X. Lin, J. Song, X. Chen, H. Yang, *Angew. Chem., Int. Ed.* **2020**, *59*, 14212.
57. J. Tang, C. Guha, W. A. Tomé, *Technol. Cancer Res. Treat.* **2015**, *14*, 221.
58. Y. T. Didenko, K. S. Suslick, *Nature* **2002**, *418*, 394.
59. Y. Nosaka, A. Y. Nosaka, *Chem. Rev.* **2017**, *117*, 11302.
60. S. Tojo, T. Tachikawa, M. Fujitsuka, T. Majima, *Chem. Phys. Lett.* **2004**, *384*, 312.
61. Y. Li, J. Xie, W. Um, D. G. You, S. Kwon, L. Zhang, J. Zhu, J. H. Park, *Adv. Funct. Mater.* **2021**, *31*, 2008061.
62. C. J. Wang, W. Li, *Drug Dev. Res.* **2016**, *77*, 152.
63. K. Wang, C. Han, J. Li, J. Qiu, J. Sunarso, S. Liu, *Angew. Chem., Int. Ed.* **2022**, *61*, e202110429.
64. D. J. Flannigan, K. S. Suslick, *Nature* **2005**, *434*, 52.
65. X. Zhou, S. Wu, C. Li, F. Yan, H. Bai, B. Shen, H. Zeng, J. Zhai, *Nano Energy* **2019**, *66*, 104127.
66. X. Chen, Y. Li, X. Pan, D. Cortie, X. Huang, Z. Yi, *Nat. Commun.* **2016**, *7*, 12273.

67. Y. Wang, X. Wen, Y. Jia, M. Huang, F. Wang, X. Zhang, Y. Bai, G. Yuan, Y. Wang, *Nat. Commun.* **2020**, *11*, 1328.
68. H. S. Xia, Z. H. Wang, *Science* **2019**, *366*, 1451.
69. K. Kubota, Y. Pang, A. Miura, H. Ito, *Science* **2019**, *366*, 1500.
70. Z. L. Wang, *Nano Today* **2010**, *5*, 540.
71. Z. Liang, C. F. Yan, S. Rtimi, J. Bandara, *Appl. Catal., B* **2019**, *241*, 256.
72. B. Dai, G. M. Biesold, M. Zhang, H. Zou, Y. Ding, Z. L. Wang, Z. Lin, *Chem. Soc. Rev.* **2021**, *50*, 13646.
73. L. Pan, S. Sun, Y. Chen, P. Wang, J. Wang, X. Zhang, J. J. Zou, Z. L. Wang, *Adv. Energy Mater.* **2020**, *10*, 2000214.
74. X. Wan, Y. Zhao, Z. Li, L. Li, *Exploration* **2022**, *2*, 20210029.
75. I. Hussain, Y. Zhang, M. Li, S. Huang, W. Hayat, L. He, X. Du, G. Liu, M. Du, *Catal. Today* **2018**, *310*, 130.
76. F. Mushtaq, X. Chen, H. Torlakcik, C. Steuer, M. Hoop, E. C. Siringil, X. Marti, G. Limburg, P. Stipp, B. J. Nelson, S. Pané, *Adv. Mater.* **2019**, *31*, 1901378.
77. Y. Zhang, Y. Leng, M. Willatzen, B. Huang, *MRS Bull.* **2018**, *43*, 928.
78. D. Tan, Y. Xiang, Y. G. Leng, Y. S. Leng, *Nano Energy* **2018**, *50*, 291.
79. S. Xu, L. Guo, Q. Sun, Z. L. Wang, *Adv. Funct. Mater.* **2019**, *29*, 1808737.
80. Y. Zhang, L. Yang, Y. Zhang, Z. Ding, M. Wu, Y. Zhou, C. Diao, H. Zheng, X. Wang, Z. L. Wang, *ACS Nano* **2020**, *14*, 10723.
81. Y. L. Liu, J. M. Wu, *Nano Energy* **2019**, *56*, 74.
82. L. Zhu, Z. L. Wang, *J. Phys. D: Appl. Phys.* **2019**, *52*, 343001.
83. H. Huang, J. Zhao, Y. Du, C. Zhou, M. Zhang, Z. Wang, Y. Weng, J. Long, J. Hofkens, J. A. Steele, M. B. J. Roeffaers, *ACS Nano* **2020**, *14*, 16689.
84. Z. Zhou, S. Yuan, J. Wang, *Front. Phys.* **2021**, *16*, 43203.
85. Y. Chen, L. Wang, R. Gao, Y. C. Zhang, L. Pan, C. Huang, K. Liu, X. Y. Chang, X. Zhang, J. J. Zou, *Appl. Catal., B* **2019**, *259*, 118079.
86. H. Li, W. Tu, Y. Zhou, Z. Zou, *Adv. Sci.* **2016**, *3*, 1500389.
87. P. Zhou, J. Yu, M. Jaroniec, *Adv. Mater.* **2014**, *26*, 4920.
88. H. Shibaguchi, H. Tsuru, M. Kuroki, *Anticancer Res.* **2011**, *31*, 2425.
89. W. Yue, L. Chen, L. Yu, B. Zhou, H. Yin, W. Ren, C. Liu, L. Guo, Y. Zhang, L. Sun, K. Zhang, H. Xu, Y. Chen, *Nat. Commun.* **2019**, *10*, 2025.
90. P. Zhu, Y. Chen, J. Shi, *Adv. Mater.* **2020**, *32*, 2001976.
91. Y. Zhao, S. Wang, Y. Ding, Z. Zhang, T. Huang, Y. Zhang, X. Wan, Z. L. Wang, L. Li, *ACS Nano* **2022**, *16*, 9304.
92. S. Cheng, Y. Luo, J. Zhang, R. Shi, S. Wei, K. Dong, X. Liu, S. Wu, H. Wang, *Chem. Eng. J.* **2022**, *442*, 136380.
93. Z. Li, T. Zhang, F. Fan, F. Gao, H. Ji, L. Yang, *J. Phys. Chem. Lett.* **2020**, *11*, 1228.
94. Y. Dong, S. Dong, B. Liu, C. Yu, J. Liu, D. Yang, P. Yang, J. Lin, *Adv. Mater.* **2021**, *33*, 2106838.
95. Y. Kang, Z. Mao, Y. Wang, C. Pan, M. Ou, H. Zhang, W. Zeng, X. Ji, *Nat. Commun.* **2022**, *13*, 2425.
96. J. Ouyang, L. Deng, W. Chen, J. Sheng, Z. Liu, L. Wang, Y. N. Liu, *Chem. Commun.* **2018**, *54*, 2874.
97. Y. Liu, Y. Wang, W. Zhen, Y. Wang, S. Zhang, Y. Zhao, S. Song, Z. Wu, H. Zhang, *Biomaterials* **2020**, *251*, 120075.
98. Q. T. Hoang, V. Ravichandran, T. G. N. Cao, J. H. Kang, Y. T. Ko, T. I. Lee, M. S. Shim, *Chem. Eng. J.* **2022**, *435*, 135039.
99. H. Ge, J. Du, J. Zheng, N. Xu, Q. Yao, S. Long, J. Fan, X. Peng, *Chem. Eng. J.* **2022**, *446*, 137040.
100. Y. Kang, L. Lei, C. Zhu, H. Zhang, L. Mei, X. Ji, *Mater. Horiz.* **2021**, *8*, 2273.
101. J. Lei, C. Wang, X. Feng, L. Ma, X. Liu, Y. Luo, L. Tan, S. Wu, C. Yang, *Chem. Eng. J.* **2022**, *435*, 134624.
102. M. Wu, Z. Zhang, Z. Liu, J. Zhang, Y. Zhang, Y. Ding, T. Huang, D. Xiang, Z. Wang, Y. Dai, X. Wan, S. Wang, H. Qian, Q. Sun, L. Li, *Nano Today* **2021**, *37*, 101104.
103. W. Ma, M. Lv, F. Cao, Z. Fang, Y. Feng, G. Zhang, Y. Yang, H. Liu, *J. Environ. Chem. Eng.* **2022**, *10*, 107840.
104. Q. Bai, J. Zhang, Y. Yu, C. Zhang, Y. Jiang, D. Yang, M. Liu, L. Wang, F. Du, N. Sui, Z. Zhu, *ACS Appl. Mater. Interfaces* **2022**, *14*, 26455.
105. X. Feng, L. Ma, J. Lei, Q. Ouyang, Y. Zeng, Y. Luo, X. Zhang, Y. Song, G. Li, L. Tan, X. Liu, C. Yang, *ACS Nano* **2022**, *16*, 2546.
106. S. Son, J. H. Kim, X. Wang, C. Zhang, S. A. Yoon, J. Shin, A. Sharma, M. H. Lee, L. Cheng, J. Wu, J. S. Kim, *Chem. Soc. Rev.* **2020**, *49*, 3244.
107. K. Ai, J. Huang, Z. Xiao, Y. Yang, Y. Bai, J. Peng, *Mater. Today Chem.* **2021**, *20*, 100402.
108. P. Zhao, Y. Jiang, Z. Tang, Y. Li, B. Sun, Y. Wu, J. Wu, Y. Liu, W. Bu, *Angew. Chem., Int. Ed.* **2021**, *60*, 8905.
109. L. Cheng, S. Qiu, J. Wang, W. Chen, J. Wang, W. Du, L. Song, Y. Hu, *Colloids Surf., A* **2022**, *638*, 128284.
110. T. Chen, W. Zeng, C. Tie, M. Yu, H. Hao, Y. Deng, Q. Li, H. Zheng, M. Wu, L. Mei, *Bioact. Mater.* **2022**, *10*, 515.
111. O. Planas, N. Macia, M. Agut, S. Nonell, B. Heyne, *J. Am. Chem. Soc.* **2016**, *138*, 2762.
112. J. Wang, L. Sui, J. Huang, L. Miao, Y. Nie, K. Wang, Z. Yang, Q. Huang, X. Gong, Y. Nan, K. Ai, *Bioact. Mater.* **2021**, *6*, 4209.
113. Y. Ding, Y. Dai, M. Wu, L. Li, *Chem. Eng. J.* **2021**, *426*, 128880.
114. L. Liang, X. Kang, Y. Sang, H. Liu, *Adv. Sci.* **2016**, *3*, 1500358.
115. W. Lei, T. Zhang, P. Liu, J. A. Rodriguez, G. Liu, M. Liu, *ACS Catal.* **2016**, *6*, 8009.
116. S. Kawasaki, R. Takahashi, T. Yamamoto, M. Kobayashi, H. Kumigashira, J. Yoshinobu, F. Komori, A. Kudo, M. Lippmaa, *Nat. Commun.* **2016**, *7*, 11818.
117. D. K. Mills, U. Jammalamadaka, K. Tappa, J. Weisman, *Bioact. Mater.* **2018**, *3*, 157.
118. S. H. Jung, C. M. Ryu, J. S. Kim, *J. Microbiol.* **2019**, *57*, 829.
119. L. Serpe, F. Giuntini, *J. Photochem. Photobiol., B* **2015**, *150*, 44.
120. S. Masimukku, Y. C. Hu, Z. H. Lin, S. W. Chan, T. M. Chou, J. M. Wu, *Nano Energy* **2018**, *46*, 338.
121. W. Zhen, Y. Liu, X. Jia, L. Wu, C. Wang, X. Jiang, *Nanoscale Horiz.* **2019**, *4*, 720.
122. R. Chauhan, G. K. Dinesh, B. Alawa, S. Chakma, *Chemosphere* **2021**, *277*, 130324.
123. P. Wang, C. Li, X. Wang, W. Xiong, X. Feng, Q. Liu, A. W. Leung, C. Xu, *Ultrason. Sonochem.* **2015**, *23*, 116.
124. Y. Kim, H. S. Lee, K. H. Son, J. W. Lee, Y. G. Lee, *Photodiagn. Photodyn. Ther.* **2017**, *17*, A56.
125. F. Alves, G. G. Guimarães, N. M. Inada, S. Pratavieira, V. S. Bagnato, C. Kurachi, *Lasers Surg. Med.* **2021**, *53*, 1113.

AUTHOR BIOGRAPHIES

Yunchao Zhao received his M.S. degree from Qingdao University in 2017. He is currently a Ph.D. candidate in Guangxi University and a joint student of Prof. Linlin Li's group in Beijing Institute of Nanoenergy and Nanosystems, CAS. His research focuses on nanomaterials for cancer theranostics and biomedical applications.

Tian Huang received her B.S. degree from Qingdao University in 2018. She joined the Beijing Institute of Nanoenergy and Nanosystems in 2019 as a joint student of Prof. Linlin Li's group, and received the M.S. degree from Guangxi University in 2022. Her research focuses on piezoelectric nanomaterials in sonodynamic therapy.

Dr. Xiaodi Zhang received her Ph. D. degree in Nanoscience and Technology from National Center for Nanoscience and Technology in 2019. She is a postdoctoral fellow in Johns Hopkins University School of Medicine. Her research interests are the role and pathology of air pollution in the induction of neurodegenerative diseases and the tissue engineering-based therapy for neurodegenerative diseases.

Dr. Yuanbo Cui received his Ph.D. degree in Biophysics from the Institute of Biophysics, Chinese Academy of Sciences in 2005. He completed his Postdoctoral research at UC-Berkeley in 2011, and later worked as a research scientist at Stanford University. Currently, he works at Santa Clara University. His research interests include single molecule biophysics, development of biosensor in early cancer detection and therapy.

Lili Zhang received her M.D. degree in Clinical Medicine from Central South University in 2017. She is currently undergoing residency training in Internal Medicine at HCA Florida Healthcare Westside/Northwest Hospital Internal Medicine program. Her research interests are cancer diagnosis, tumor biomarkers and biosensors.

Prof. Linlin Li received her Ph.D. degree in Physical Chemistry from the Technical Institute of Physics and Chemistry, Chinese Academy of Sciences in 2008. Currently, she is a professor and group leader at Beijing Institute of Nanoenergy and Nanosystems, CAS. She has been awarded the National Youth Talent Support Program and CAS Lu Jiaxi Award for Young Talents. She has authored over 140 peer-reviewed papers and 3 book chapters. Her research interests mainly include biomedical application of biomaterials and self-powered devices in cancer therapy, biosensing, and tissue regeneration. Details can be found at: https://www.x-mol.com/groups/lilinlin.

Prof. Zhong Lin Wang is the Hightower Chair in Materials Science and Engineering and Regents' Professor at Georgia Tech and the Chief Scientist and Director of the Beijing Institute of Nanoenergy and Nanosystems, Chinese Academy of Sciences. His discovery and breakthroughs in developing nanogenerators and self-powered nanosystems establish the principle and technological road map for harvesting mechanical energy from environmental and biological systems for powering personal electronics and future sensor networks. He pioneered the field of piezotronics and piezo-phototronics.

How to cite this article: Y. Zhao, T. Huang, X. Zhang, Y. Cui, L. Zhang, L. Li, B. Li, Z. L. Wang, *BMEMat* **2023**, e12006. https://doi.org/10.1002/bmm2.12006